Progress In Electromagnetics Research Letters, Vol. 50, 19–27, 2014

Analysis of MM-Wave Bands Quasi-Optical Unstable Bessel-Gauss Resonator by IDGF Algorithm

Yanzhong Yu[1, 2, *], Hongfu Meng[2], and Wenbin Dou[2]

Abstract—An analysis of quasi-optical unstable Bessel-Gauss resonator (QOUBGR) at millimeter wavelengths is presented in this paper. The QOUBGR, formed by a conical mirror and a convex mirror, is designed on the basic of quasi-optical theory and techniques. For the purpose of precisely analyzing the designed QOUBGR, a new algorithm known as iterative dyadic Green's functions (IDGF) is proposed, which originates from famous Fox-Li algorithm. The IDGF algorithm can calculate not only two-dimension (2-D) but also three-dimension (3-D) resonating modes in the cavity. Simulation results demonstrate that the designed QOUBGR can steadily support both zero-order and high-order resonant modes that are approximations to Bessel-Gauss beams. These beams will find their promising applications in the MM- and/or quasi-optical imaging and measurement systems.

1. INTRODUCTION

A Bessel beam was first introduced into optics by Durnin and coworker in 1987 [1, 2]. Subsequently, a Bessel-Gauss beam was also proposed by Gori et al. in the same year [3]. These Bessel-type beams own many novel characteristics, such as extremely narrow transverse of intensity, excessively large depth of field, and very long range of propagation. Therefore, lots of potential applications can be found in physics, chemistry, biology, and engineering, for instance, imaging [4, 5], micromanipulation [6, 7], and measurements [8]. From then on, the research of effective generation of these beams has attracted much attention in the world. As a result, a large number of approaches to produce Bessel or Bessel-Gauss beams have been reported [9–11]. Up to now, the proposed methods can be roughly categorized into passive and active schemes [12–14]. When compared with the passive scheme that needs an optical element to transform an incident beam into a Bessel or Bessel-Gauss beam, the active one has the advantages of improving quality and achieving frequency conversion of output beam, which commonly utilizes a cavity to directly generate a Bessel or Bessel-Gauss mode. Hence the latter has become a popular way to create the Bessel or Bessel-Gauss beam [15–18]. Additionally, the Bessel-Gauss beam is easier to be produced than the Bessel beam, since the ideal Bessel beam owns an infinite bound in the cross section and possesses an infinite amount of energy [14].

In the previous work, the Bessel resonator [19] and stable Bessel-Gauss resonator [20] were analyzed by using ISCF (iterative Stratton-Chu formula) algorithm. In the present paper, we report our latest research result. A QOUBGR at mm-wave bands is formed by using quasi-optical theory and techniques. In order to exactly evaluate the resonating mode of the designed QOUBGR, a new algorithm, named as IDGF algorithm, is exploited based on the classical Fox-Li algorithm. The IDGF algorithm, which uses dyadic Green's function to evaluate the diffractive field in the cavity, is more rigorous than the ISCF algorithm that employs Stratton-Chu formula to calculate the resonating mode. Moreover, it can analyze not only 2-D but also 3-D resonant modes in the cavity, but the ISCF algorithm can compute only 2-D distribution. Simulation results indicate that the designed QOUBGR can stably support

Received 3 October 2014, Accepted 6 November 2014, Scheduled 12 November 2014

* Corresponding author: Yan-Zhong Yu (yuyanzhong059368@gmail.com).

[1] College of Physics & Information Engineering, Quanzhou Normal University, Fujian 362000, China. [2] State Key Lab of Millimeter Waves, Southeast University, Nanjing 210096, China.

both zero-order and high-order resonant modes which are approximations to Bessel-Gauss beams. The beams generated from the designed QOUBGR may find their potential applications in the mm- and/or quasi-optical systems [21].

The rest of the present paper is organized as follows. A design of QOUBGR is described in Section 2. Section 3 introduces the IDGF algorithm in detail. Analysis results of the designed QOUBGR are presented in Section 4. A brief summary is given in Section 5.

2. QOUBGR DESIGN

To conveniently introduce the design principle of QOUBGR, we must first recognize the Bessel and Bessel-Gauss beams. In the cylindrical coordinates system, an ideal mth-order Bessel beam can be given by [1, 2]

$$U_{BB}(\rho,\varphi,z) = U_0 J_m(k_\perp \rho)\exp[i(k_z z + m\varphi) \tag{1}$$

Then the mth-order Bessel-Gauss beam in the paraxial condition can be approximated by [15]

$$\begin{aligned} U_{BGB}(\rho,\varphi,z) \;=\; & U_0 \frac{w_0}{w(z)} J_m\left(\frac{k_\perp \rho}{1+iz/z_R}\right)\exp\left\{-\left[\frac{1}{w^2(z)}-\frac{ik}{2R_g(z)}\right]\right. \\ & \left.\times\left(\rho^2+\theta^2 z^2\right)\right\}\exp(i\Phi(z))\exp(im\varphi) \end{aligned} \tag{2}$$

The mth-order Bessel-Gauss beam at its waist ($z = 0$) may be simplified as [3, 22]

$$U_{BGB}(\rho,\varphi,z=0) = U_0 J_m(k_\perp \rho)\exp(im\varphi)\exp(-\rho^2/w_0^2) \tag{3}$$

where the subscripts BB and BGB identify the Bessel and Bessel-Gauss beam, respectively. U_0 is a constant and J_m the mth-order Bessel function of the first kind. ρ, φ, and z are the radial, azimuthal, and longitudinal coordinates, respectively, $\rho^2 = x^2 + y^2$. $k_\perp^2 + k_z^2 = k^2 = (2\pi/\lambda)^2$, $k_\perp$ and k_z represent respectively the radial and axial wave numbers, $k_\perp = k\sin\theta$. θ is the conical angle of the Bessel beam, λ a wavelength in free space, and w_0 the waist radius of the corresponding Gaussian beam. $w(z) = w_0[1+(z/z_R)^2]^{1/2}$ represents the radius of Gaussian beam propagating to the distance z from its waist ($z = 0$). $z_R = kw_0^2/2$ denotes the Rayleigh range of the beam, $\Phi(z) = k(1-\theta^2/2)z - \arctan(z/z_R)$ the axial phase of the Bessel-Gauss beam, and $R_g(z) = z + z_R^2/z$ the wave-front curvature of Gaussian beam.

Figure 1 illustrates the 3-D intensity distributions for Bessel beam and Bessel-Gauss beam at its waist ($z = 0$), respectively. The zero-order Bessel and Bessel-Gauss beams have a maximum intensity at the center, but at the same place the intensity distributions of high-order Bessel and Bessel-Gauss beams are null. It can be observed from Fig. 1 that the radial distribution of an ideal Bessel beam extends to infinite far, but the scope of radial extension of Bessel-Gauss beam is limited, due to the modulation of Gaussian function. Therefore, the generation of approximation to Bessel-Gauss beam may be much easier theoretically and experimentally than that of Bessel beam. The phase distributions of zero-order and high-order Bessel-Gauss beams at their waists are shown in Fig. 2, in which one can see that the phase distribution of zero order is circularly symmetric but that of high order exhibits odd symmetry about the central point, however, both are ring-shaped profiles.

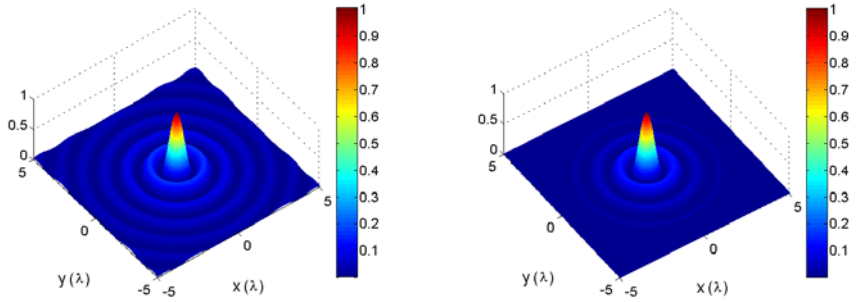

(a) (b)

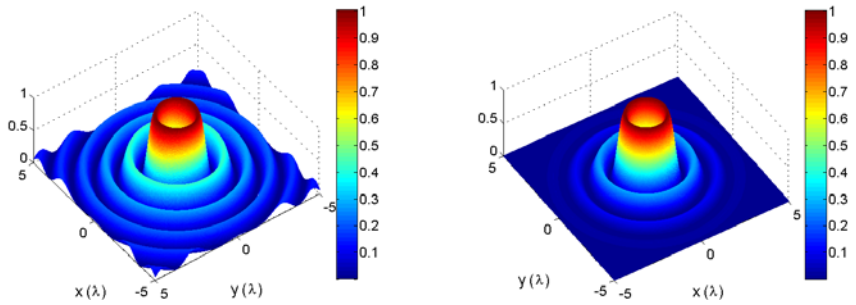

Figure 1. 3-D Intensity distributions for (a) zero-order Bessel beam, (b) zero-order Bessel-Gauss beam at its waist ($z = 0$), (c) second-order Bessel beam, and (d) second-order Bessel-Gauss beam at its waist ($z = 0$). The relevant parameters are: $\lambda = 3\,\text{mm}$, $w_0 = 4.545\lambda$, $k_\perp = 2.886/\lambda$, and $\rho = 5\lambda$.

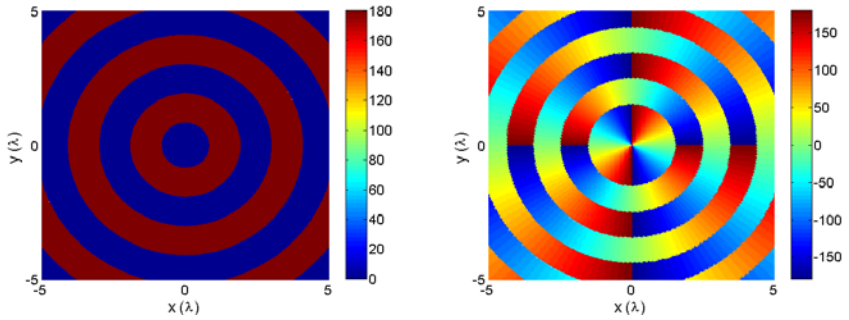

Figure 2. Top views of phase distributions of Bessel-Gauss beams at their waists ($z = 0$). (a) zero order, and (b) second order. All parameters are the same as in Fig. 1.

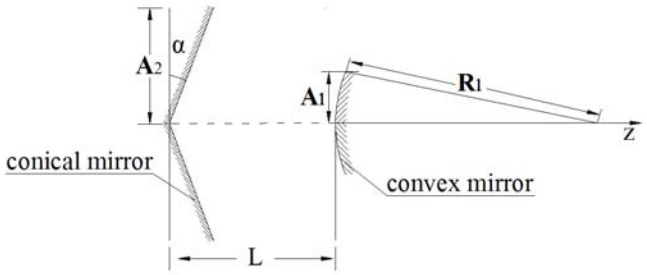

Figure 3. Schematic diagram of the QOUBGR composed of a conical mirror and a convex spherical mirror.

When comparing Eq. (1) with Eq. (3), the mth-order Bessel-Gauss beam at its waist may be explained as the mth-order Bessel beam modulated by a Gaussian function. Accordingly, the wavefront of Bessel-Gauss beam can be considered as a superposition of conical wavefront of Bessel beam and spherical wavefront of Gaussian beam. It is known that if one wants to obtain some field expected, he may form a resonator with end mirror that conjugates the radial phase of this field [15]. Therefore, to produce Bessel-Gauss beam, we can design a resonator that consists of a conical mirror and a spherical mirror. Provided that the spherical mirror is concave, one can form a quasi-optical stable Bessel-Gauss cavity [20]. On the contrary, a convex spherical mirror can be employed to model a quasi-optical unstable Bessel-Gauss resonator (QOUBGR), as illustrated in Fig. 3. The base planes of conical mirror and convex spherical mirror are perfectly reflective; therefore the electromagnetic wave in the cavity can round trip propagate and excite the resonating mode. The related parameters of the QOUBGR

are: α represents the conical angle of conical mirror, A_1 and A_2 denote respectively the aperture radii of conical mirror and convex mirror, and $A_2 = 2A_1$, R_1 is the radius of curvature of convex mirror. The cavity length L between conical and convex mirrors can be computed by [13, 16, 17]

$$L = \frac{R_2}{2\tan\alpha} \tag{4}$$

3. IDGF ALGORITHM

It is well known that the optic resonator can be analyzed by the famous Fox-Li algorithm, which was first proposed by Fox and Li in 1960 [23]. The Kirchhoff scalar diffraction theory is used to calculate diffraction field of the resonator in Fox-Li iterative algorithm. The validity of Kirchhoff theory is based on several assumptions, of which the following are the most important: the numerical aperture (NA) is rationally small; the Fresnel number is very large; and the incident radiation is unpolarized [24]. Violation of any of these three assumptions can make the Kirchhoff analysis invalidated. Unlike the optical elements or systems, at mm-wave bands these elements or systems can no longer satisfy simultaneously the constraints mentioned above. Consequently, the Fox-Li algorithm is unfit to analyze the resonator at millimeter wavelengths. To conquer this problem, in our previous work [19, 20], we had developed an iterative method named as ISCF algorithm, in which the Stratton-Chu formula is utilized to calculate the electromagnetic field in the resonator. On the foundation of the ISCF algorithm, now we develop a new program called as IDGF algorithm to further improve analysis precision of the cavity. In addition, this algorithm has an important characteristic of calculating 3-D resonant mode when compared with the 2-D ISCF algorithm.

The IDGF algorithm employs the dyadic Green's function to compute the diffraction field inside the cavity. The dyadic Green's function theory is an extremely powerful and efficient way in the study of electromagnetic wave propagation and scattering, and has been extensively developed to solve so many electromagnetic problems [25–30]. The electric and magnetic field components $\vec{E}$ and $\vec{H}$ of the dyadic Green's function diffraction integral formula can be written as [25]

$$\vec{E}(\vec{r}) = \int_{S'} \bar{\bar{G}}_{ee}(\vec{r},\vec{r}')\,\vec{J}(\vec{r}')\,dS' + \int_{S'} \bar{\bar{G}}_{em}(\vec{r},\vec{r}')\vec{M}(\vec{r}')\,dS' \tag{5}$$

$$\vec{H}(\vec{r}) = \int_{S'} \bar{\bar{G}}_{me}(\vec{r},\vec{r}')\,\vec{J}(\vec{r}')\,dS' + \int_{S'} \bar{\bar{G}}_{mm}(\vec{r},\vec{r}')\vec{M}(\vec{r}')\,dS' \tag{6}$$

Or in matrix form

$$\begin{bmatrix} \vec{E}(\vec{r}) \\ \vec{H}(\vec{r}) \end{bmatrix} = \int_{S'} \begin{bmatrix} \bar{\bar{G}}_{ee}(\vec{r},\vec{r}') & \bar{\bar{G}}_{em}(\vec{r},\vec{r}') \\ \bar{\bar{G}}_{me}(\vec{r},\vec{r}') & \bar{\bar{G}}_{mm}(\vec{r},\vec{r}') \end{bmatrix} \cdot \begin{bmatrix} \vec{J}(\vec{r}') \\ \vec{M}(\vec{r}') \end{bmatrix} dS' \tag{7}$$

where

$$\bar{\bar{G}}_{ee}(\vec{r},\vec{r}') = -j\omega\mu\bar{\bar{G}}_e(\vec{r},\vec{r}')$$

$$\bar{\bar{G}}_{mm}(\vec{r},\vec{r}') = -j\omega\varepsilon\bar{\bar{G}}_e(\vec{r},\vec{r}')$$

$$\bar{\bar{G}}_{em}(\vec{r},\vec{r}') = -\bar{\bar{G}}_{me}(\vec{r},\vec{r}') = -\bar{\bar{G}}_m(\vec{r},\vec{r}')$$

$$\bar{\bar{G}}_m(\vec{r},\vec{r}') = \left(\frac{1}{R} + jk\right) \begin{bmatrix} 0 & u_z & -u_y \\ -u_z & 0 & u_x \\ u_y & -u_x & 0 \end{bmatrix} G_0(\vec{r},\vec{r}')$$

$$\bar{\bar{G}}_e(\vec{r},\vec{r}') = \begin{bmatrix} Pu_xu_x + Q & Pu_xu_y & Pu_xu_z \\ Pu_yu_x & Pu_yu_y + Q & Pu_yu_z \\ Pu_zu_x & Pu_zu_y & Pu_zu_z + Q \end{bmatrix} G_0(\vec{r},\vec{r}')$$

$$P = \frac{3}{k^2R^2} + j\frac{3}{kR} - 1, \quad Q = -\frac{1}{k^2R^2} - j\frac{1}{kR} + 1$$
$$G_0\left(\vec{r},\vec{r}'\right) = \frac{e^{-jk|\vec{r}-\vec{r}'|}}{4\pi\left|\vec{r}-\vec{r}'\right|}, \quad u_x = \frac{x-x'}{R}, \quad u_y = \frac{y-y'}{R}, \quad u_z = \frac{z-z'}{R}$$
$$R = \sqrt{(x-x')^2 + (y-y')^2 + (z-z')^2}$$
$$\vec{J}\left(\vec{r}'\right) = \vec{n} \times \vec{H}, \quad \vec{M}\left(\vec{r}'\right) = \vec{E} \times \vec{n}$$

$\bar{\bar{G}}_{ee}\left(\vec{r},\vec{r}'\right)$ and $\bar{\bar{G}}_{mm}\left(\vec{r},\vec{r}'\right)$ are called respectively electric and magnetic type dyadic Green's functions; $\bar{\bar{G}}_{em}\left(\vec{r},\vec{r}'\right)$ and $\bar{\bar{G}}_{me}\left(\vec{r},\vec{r}'\right)$ are called respectively electric-magnetic type and magneticelectric type dyadic Green's functions; $G_0\left(\vec{r},\vec{r}'\right)$ is the free-space scalar Green's function. $\vec{r}(x,y,z)$ and $\vec{r}'(x',y'z')$ are an arbitrary observation point in the far region and an source point on the integral surface S', respectively. ω and ε denote the angular frequency and the permittivity, respectively. $\vec{J}\left(\vec{r}'\right)$ and $\vec{M}\left(\vec{r}'\right)$ mark respectively electric and magnetic current density on the surface. Unit vector $\vec{n}$ is the outer normal of the integral surface S'.

When Eq. (6) is utilized to compute the electromagnetic fields diffracted by a perfectly conducting surface, the boundary conditions of $\vec{n} \times \vec{E} = 0$ on perfectly conducting surface must be considered. Then Eq. (6) can be simplified by

$$\vec{H}\left(\vec{r}\right) = \int_{S'} \bar{\bar{G}}_m \vec{J}\left(\vec{r}'\right) dS' = \int_{S'} \bar{\bar{G}}_m \overrightarrow{n} \times \overrightarrow{H}\left(\vec{r}'\right) dS' = \int_{S'} \bar{\bar{G}}_m 2\vec{n} \times \vec{H}_i\left(\vec{r}'\right) dS' \tag{8}$$

In which the fact that $\vec{n} \times \vec{H}\left(\vec{r}'\right) = 2\vec{n} \times \vec{H}_i\left(\vec{r}'\right)$ on the perfectly conducting surface is used, and $\vec{H}_i$ represents the incident magnetic field vector.

According to resonator theory, the steady-state field will be obtained after electromagnetic wave round trip propagates enough times in the cavity. Its relative distribution is not affected by the diffraction, and it can be self-reproduction after round trip propagating. The only thing that seems to change is that its amplitudes attenuate on the same proportion and its phases delay on the same size. This steady-state field is also called as self-reproduction mode [31].

The process of IDGF algorithm corresponds to that of electromagnetic wave round-trip propagation in the cavity. As depicted schematically in Fig. 4, in order to describe easily and compute handily, we split one round-trip propagation into two one-way transits. At the first transit, assuming that the initial

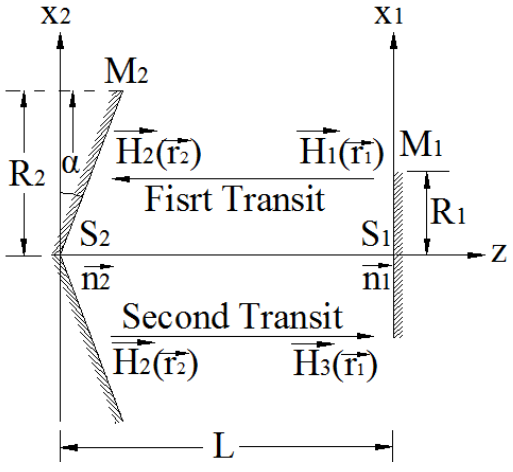

Figure 4. Schematic for the improved IDGF algorithm. S_1 and S_2 represent respectively the inner surfaces of the mirrors M_1 and M_2; unit vector $\vec{n}_1$ and $\vec{n}_2$ denote the outer normal of the S_1 and S_2, respectively; R_1 and R_2 are the aperture radii of the M_1 and M_2, respectively; L is the cavity length and α is the conical angel of the mirror M_2; H_{q+1} marks the field distribution after the qth-time transit.

field $\vec{H}_1(\vec{r}_1)$ on the mirror M_1 propagates to the mirror M_2, the diffraction field $\vec{H}_2(\vec{r}_2)$ on the mirror M_2 may be calculated by Eq. (8)

$$\vec{H}_2(\vec{r}_2) = \int_{S_1'} \bar{G}_{m1} 2\vec{n}_1 \times \vec{H}_1(\vec{r}_1)\, dS_1' \tag{9}$$

At the second transit, from mirror M_2 to mirror M_1, the field $\vec{H}_3(\vec{r}_1)$ can be obtained by

$$\vec{H}_3(\vec{r}_1) = \int_{S_2'} \bar{G}_{m2} 2\vec{n}_2 \times \vec{H}_2(\vec{r}_2)\, dS_2' \tag{10}$$

Based on the self-reproduction principle introduced above, a following relationship between $\vec{H}_{q-1}$ and $\vec{H}_{q+1}$ can be obtained after q times transit (q enough large).

$$\vec{H}_{q+1} = \frac{1}{\gamma}\vec{H}_{q-1} \tag{11}$$

where $\vec{H}$ denotes the eigen field distribution on the mirror M_1 or M_2; γ is the complex eigen value independent of the position coordinate, which defines the fractional power loss per round trip

$$\delta = 1 - \left|\frac{1}{\gamma}\right|^2 \tag{12}$$

and the additional phase shift per round trip

$$\Phi = \arg\frac{1}{\gamma} \tag{13}$$

The procedure of executing IDGF algorithm can be summarized to four main steps: (A) supposing there exists an initial field distribution $\vec{H}_1(\vec{r}_1)$ on the mirror M_1, in general, the arbitrary initial distribution is permitted; (B) substitution of $\vec{H}_1(\vec{r}_1)$ into Eq. (9) yields $\vec{H}_2(\vec{r}_2)$ on the mirror M_2; (C) normalizing $\vec{H}_2(\vec{r}_2)$, i.e., $|\vec{H}_2(\vec{r}_2)|_{\max} = 1$, and then substituting it into Eq. (10), obtains $\vec{H}_3(\vec{r}_1)$ on the mirror M_1; (D) repeating this iterative process until the relative field distribution reaches a steady state that satisfies Eq. (11). The obtained field distribution can be regarded as an iterative normal mode of the resonator [23].

4. ANALYSIS RESULTS

The QOUBGR can be easily designed according to the configuration of resonator illustrated in Fig. 3. The relevant parameters for the simulated QOUBGR in the present work are as follows: $R_2 = 60\,\text{mm}$; $R_1 = R_2/2 = 30\,\text{mm}$; $\alpha = 22.38°$; $R = 1165.5\,\text{mm}$; $L = 72.8\,\text{mm}$; $\lambda = 8\,\text{mm}$. Now, supposing that there exists an uniform plane wave on the aperture of convex mirror M_1, i.e., $\vec{H}_1(x_1, y_1, z_1) = \vec{y}$, then executing the IDGF algorithm and through 60 times of transition, the electromagnetic field distribution inside the cavity approaches a steady state, that is, satisfying the convergence condition of Eq. (11) and then the resonating mode can be acquired. Figs. 5(a) and(b) show the 3-D intensity and phase distributions of the foundational mode (zero-order mode) on the convex mirror M_1. It can be observed easily from Fig. 5(a) that the maximum value of normalized intensity locates at the center of the convex mirror, and the radial distribution extends in a limited range. From Fig. 5(b) one can find that the phase distribution exhibits circular symmetry and shows a ring-shaped profile. Comparing Fig. 5(a) and Fig. 5(b) with Fig. 1(a) and Fig. 2(a), respectively, one can infer that the resonant mode is an approximation to zero-order Bessel-Gauss beam, known as the pseudo Bessel-Gauss beam [20].

In order to generate high-order mode, for example, first-order mode, one should change the initial exciting field distribution. Provided that $\vec{H}_1(x_1 \geq 0, y_1, z_1) = \vec{y}$, and $\vec{H}_1(x_1 < 0, y_1, z_1) = -\vec{y}$ on the convex mirror, we can obtain finally the first-order mode, as illustrated in Fig. 6. Unlike the zero-order mode, the first-order mode has a minimum intensity at the center of convex mirror, and its phase distribution is odd-symmetric about center point and still displays a ring-shape profile.

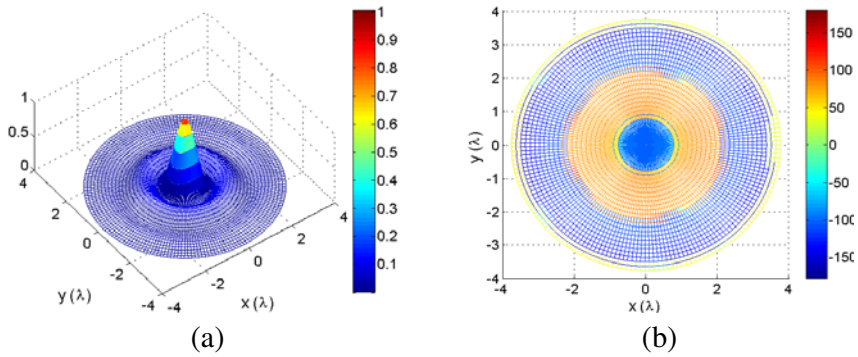

Figure 5. 3-D distributions of zero-order resonating mode on the convex mirror M_1. (a) 3-D normalized intensity, and (b) top view of phase distribution.

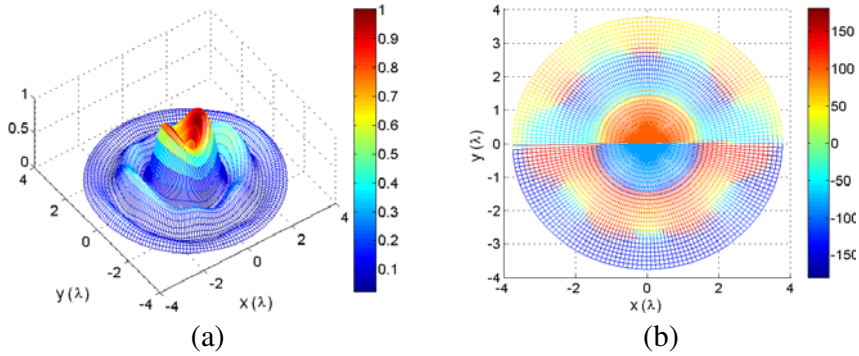

Figure 6. 3-D distributions of first-order resonating mode on the convex mirror. (a) 3-D normalized intensity, and (b) top view of phase distribution.

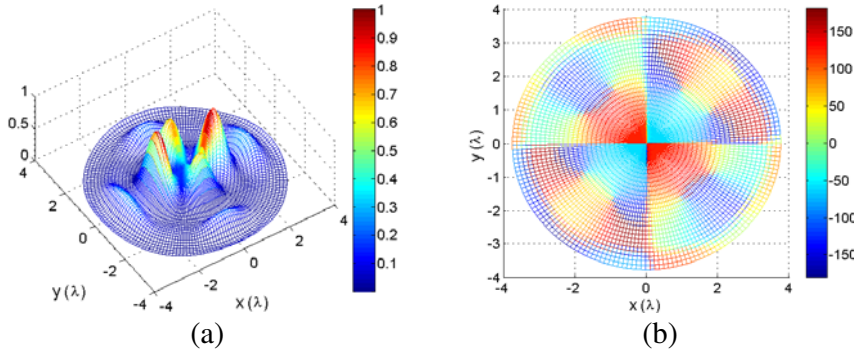

Figure 7. 3-D distributions of second-order mode on the convex mirror. (a) 3-D normalized intensity, and (b) top view of phase distribution.

Additionally, if an initial field distribution on the convex mirror M_1 is presented as: $\vec{H}_1(x_1 \geq 0, y_1 \geq 0, z_1) = \vec{y}$, $\vec{H}_1(x_1 < 0, y_1 \geq 0, z_1) = -\vec{y}$, $\vec{H}_1(x_1 < 0, y_1 < 0, z_1) = \vec{y}$, $\vec{H}_1(x_1 \geq 0, y_1 < 0, z_1) = -\vec{y}$, the second-order resonating mode can be excited, as shown in Fig. 7. The second-order mode is partly similar to the first-order mode, i.e., both modes have the same location of the minimum intensity, and their phase distributions show odd symmetry about center point and appear ring-shape profile. However, both intensity and phase distributions of the second-order mode are more complex than those of the first-order mode. By observing carefully Figs. 5(b), 6(b), and 7(b), one can find that zero-order mode has zero sector, first-order mode is two sectors, and third-order

mode owns four sectors, in other word, the mth-order mode has $2m$ sectors. This is consistent with the Bessel-Gauss beam theory.

However, it is worth pointing out that the resonating modes given in Figs. 5–7 is a little different from those illustrated in Figs. 1 and 2. This is because the observing plane is not the same. The observing plane of an ideal Bessel-Gauss beam is located at the waist of Gaussian beam, but that of the generating mode is situated at the convex mirror M_1. Another reason is that the aperture radius of the designed QOUBGR is limited, and this can also affect the distribution of resonating mode.

Finally, according to Eqs. (12) and (13), the values of the power loss and phase shift per round-trip can be computed receptively as follows: for zero-order mode, $\delta_0 = 12.75\%$ and $\Phi_0 = 135.26°$; for first-order mode, $\delta_1 = 23.88\%$ and $\Phi_1 = 141.95°$; for second-order mode, $\delta_2 = 27.04\%$ and $\Phi_2 = 305.01°$. A conclusion can be drawn from these results that the values, whether the power losses or the phase shifts, become larger as the order increases.

5. SUMMARY

The QOUBGR composed by a conical mirror and a convex mirror is designed on the basic of the quasi-optical theory and techniques. To more rigorously analyze the designed QOUBGR, we have exploited the IDGF algorithm, which employs dyadic Green's functions to evaluate the diffraction field in the cavity and can output 3-D resonant mode. A conclusion can be drawn readily from numerical results that the resonating modes in the designed QOUBGR are approximations to Bessel-Gauss beams. The potential applications of these beams will be found in the MM- and/or quasi-optical system, such as MM-wave imaging, medium parameter measurement, and remote bunching propagation of electromagnetic energy.

ACKNOWLEDGMENT

This work is supported by State Key Lab of Millimeter Waves (No. K201307), the National Natural Science Foundation of China under grant 61101020, and the Key Discipline of Electronic Science and Technology.

REFERENCES

1. Durnin, J., "Exact solutions for nondiffracting beams. I. The scalar theory," *J. Opt. Soc. Am. A*, Vol. 4, No. 4, 651–654, 1987.
2. Durnin, J., J. J. Miceli, Jr., and J. H. Eberly, "Diffraction-free beams," *Phys. Rev. Lett.*, Vol. 58, No. 15, 1499–1501, 1987.
3. Gori, F., G. Guattari, and C. Padovani, "Bessel-Gauss beams," *Opt. Commun.*, Vol. 64, No. 6, 491–495, 1987.
4. Mahon, R. J., W. Lanigan, J. A. Murphy, et al., "Novel techniques for millimeter wave imaging systems operating at 100 GHz," *Proc. SPIE Int. Soc. Opt. Eng.*, Vol. 5789, 93–100, 2005.
5. Lu, J., T. K. Song, R. R. Kinnick, et al., "In vitro and in vivo real-time imaging with ultrasonic limited diffraction beams," *IEEE Trans. Med. Imag.*, Vol. 12, No. 12, 819–829, 1993.
6. Hegner, M., "Optics: The light fantastic," *Nature*, Vol. 419, 125–127, 2002.
7. Garces-Chavez, V., D. Mcgloin, and E. H. Melvill, "Simultaneous micromanipulation in multiple planes using a self-reconstructing light beam," *Nature*, Vol. 419, 145–147, 2002.
8. Hughes, S. and J. M. Burzler, "Theory of Z-scan measurements using Gaussian-Bessel beams," *Physical Review A*, Vol. 56, No. 2, R1103–R1106, 1997.
9. Cox, A. J. and D. C. Dibble, "Nondiffracting beam from a spatially filtered Fabry-Perot resonator," *J. Opt. Soc. Am. A*, Vol. 9, No. 2, 282–286, 1992.
10. Monk, S., J. Arlt, D. A. Robertson, et al., "The generation of Bessel beams at millimetre-wave frequencies by use of an axicon," *Opt. Commun.*, Vol. 170, 213–215, 1999.
11. Meltaus, J., J. Salo, E. Noponen, et al., "Millimeter-wave beam shaping using holograms," *IEEE Trans. Microwave Theory Tech.*, Vol. 51, No. 4, 1274–1279, 2003.

12. Muys, P. and E. Vandamme, "Direct generation of Bessel beams," *Appl. Opt.*, Vol. 41, 6375–6379, 2002.
13. Hernandez-Aranda, R. I., S. Chavez-Cerda, and J. C. Gutierrez-Vega, "Theory of the unstable Bessel resonator," *J. Opt. Soc. Am. A*, Vol. 22, 1909–1917, 2005.
14. Wu, F. T., Y. B. Chen, and D. D. Guo, "Nanosecond pulsed Bessel-Gauss beam generated directly from a Nd: YAG axicon-based resonator," *Appl. Opt.*, Vol. 46, No. 22, 4943–4947, 2007.
15. Khilo, A. N., E. G. Katranji, and A. A. Ryzhevich, "Axicon-based Bessel resonator: Analytical description and experiment," *J. Opt. Soc. Am. A*, Vol. 18, No. 8, 1986–1992, 2001.
16. Rogel-Salazar, J., G. H. C. New, and S. Chávez-Cerda, "Bessel-Gauss beam optical resonator," *Opt. Commun.*, Vol. 190, 117–122, 2001.
17. Tsangaris, C. L., G. H. C. New, and J. Rogel-Salazar, "Unstable Bessel beam resonator," *Opt. Commun.*, Vol. 223, 233–238, 2003.
18. Ling, D. X. and J. C. Li, "Analysis of eigenfields in the axicon-based Bessel-Gauss resonator by the transfer-matrix method," *J. Opt. Soc. Am. A*, Vol. 23, No. 4, 912–918, 2006.
19. Yu, Y.-Z. and W.-B. Dou, "Quasi-optical Bessel resonator," *Progress In Electromagnetics Research*, Vol. 93, 205–219, 2009.
20. Yu, Y.-Z. and W.-B. Dou, "Investigation of quasi-optical Bessel-Gauss resonator at mm- and submm-wavelengths," *Progress In Electromagnetics Research*, Vol. 138, 453–466, 2013.
21. Meng, H. F., B. Xiang, J. L. Zhang, W. B. Dou, and Y. Z. Yu, "The generation of bessel beam and its application in millimeter wave imaging," *Journal of Infrared, Millimeter, and Terahertz Waves*, Vol. 35, No. 2 , 208–217, 2014.
22. Bagini, V., F. Frezza, M. Santarsiero, G. Schettini, and G. Schirripa Spagnolo, "Generalized Bessel-Gauss beams," *Journal of Modern Optics*, Vol. 43, No. 6, 1155–1166, 1996.
23. Fox, A. G. and T. Li, "Resonant modes in a maser interferometer," *Bell Syst. Tech. J.*, Vol. 40, 453–488, 1961.
24. Hsu, W. and R. Barakat, "Stratton-Chu vectorial diffraction of electromagnetic fields by apertures with application to small-Fresnel-number systems," *J. Opt. Soc. Am. A*, Vol. 11, No. 2, 623–629, 1994.
25. Eroglu, A. and J. K. Lee, "Simplified formulation of dyadic Green's functions and their duality relations for general anisotropic media," *Progress In Electromagnetics Research*, Vol. 77, 391–408, 2007.
26. Gao, G., C. Torres-Verdin, and T. M. Habashy, "Analytical techniques to evaluate the integrals of 3D and 2D spatial dyadic Green's functions," *Progress In Electromagnetics Research*, Vol. 52, 47–80, 2005.
27. Li, L.-W., N.-H. Lim, W.-Y. Yin, and J.-A. Kong, "Eigenfunctional expansion of dyadic Green's functions in gyrotropic media using cylindrical vector wave functions," *Progress In Electromagnetics Research*, Vol. 43, 101–121, 2003.
28. Hanson, G. W., A. I. Nosich, and E. M. Kartchevski, "Green's function expansions in dyadic root functions for shielded layered waveguides," *Progress In Electromagnetics Research*, Vol. 39, 61–91, 2003.
29. Li, L. W., S. B. Yeap, M. S. Leong, T. S. Yeo, and P. S. Kooi, "Dyadic Green's functions in multilayered stratified gyroelectric chiral media," *Progress In Electromagnetics Research*, Vol. 35, 53–81, 2002.
30. Tan, E. L. and S. Y. Tan, "On the eigenfunction expansions of the dyadic Green's functions for bianisotropic media," *Progress In Electromagnetics Research*, Vol. 20, 227–247, 1998.
31. Gao, Z. H., "Wave pattern property of self-reproductive mode in laser resonator," *Guangzi Xuebao/Acta Photonica Sinica*, Vol. 29, No. 8, 726–729, 2000.